Dynamic Stability Analysis of Blunt Body Entry Vehicles Using Time-Lagged Aftbody Pitching Moments

Cole D. Kazemba[1]
NASA Ames Research Center, Moffett Field, CA 94035, USA

Robert D. Braun[2]
Georgia Institute of Technology, Atlanta, Georgia 30332-0150

Mark Schoenenberger[3]
NASA Langley Research Center, Hampton, VA 23681

and

Ian G. Clark[4]
NASA Jet Propulsion Laboratory, Pasadena, CA 91109

Abstract

This analysis defines an analytic model for the pitching motion of blunt bodies during atmospheric entry. The proposed model is independent of the pitch damping sum coefficient present in the standard formulation of the equations of motion describing pitch oscillations of a decelerating blunt body, instead using the principle of a time-lagged aftbody moment as the forcing function for oscillation divergence. Four parameters, all with intuitive physical relevance, are introduced to fully define the aftbody moment and the associated time delay. It is shown that the dynamic oscillation responses typical to blunt bodies can be produced using hysteresis of the aftbody moment in place of the pitch damping coefficient. The approach used in this investigation is shown to be useful in understanding the governing physical mechanisms for blunt body dynamic stability and in guiding vehicle and mission design requirements. A validation case study using simulated ballistic range test data is conducted. From this, parameter identification is carried out through the use of a least squares optimizing routine. Results show good agreement with the limited existing literature for the parameters identified, suggesting that the model proposed could be validated by an experimental ballistic range test series. The trajectories produced by the identified parameters were found to match closely those

---

[1] Aerospace Engineer, Systems Analysis Branch, STC Inc., M/S 229-1, Member AIAA
[2] Professor, Daniel Guggenheim School of Aerospace Engineering. Fellow AIAA.
[3] Aerospace Engineer, Exploration Systems Engineering Branch, Member AIAA
[4] Aerospace Engineer, Entry, Decent, and Landing Systems and Advanced Technologies Group, Member AIAA

from the MER ballistic range tests for a wide array of initial conditions and can be identified with a
reasonable number of ballistic range shots and computational effort.

Nomenclature

A	=	Euler-Cauchy angle of attack coefficient
C_A	=	axial force coefficient
C_D	=	drag coefficient
C_L	=	lift coefficient
C_m	=	pitching moment coefficient
C_{m_α}	=	aerodynamic pitching-moment slope coefficient
$C_{m_q} + C_{m_{\dot\alpha}}$	=	aerodynamic pitch-damping sum
C_{m_q}	=	aerodynamic pitch-damping coefficient
$\overline{C_{m_q}}$	=	effective pitch damping
d	=	aerodynamic reference diameter
g	=	acceleration due to gravity
h	=	altitude
I_{yy}	=	pitch axis mass moment of inertia
l	=	characteristic length
m	=	mass
M	=	Mach number
R_p	=	planet radius
S	=	cross sectional area
t	=	time
t_{lag}	=	lag time
t^-	=	time referenced by aftbody, $t^- = t - t_{lag}$
V	=	vehicle velocity
$\mathcal{V}$	=	characteristic velocity
W	=	work over one oscillation cycle
Greek		
α	=	angle of attack
β	=	parameter of aftbody moment Mach number dependence
γ	=	flight-path angle
δ	=	phase shift constant
ε	=	residual
θ	=	pitch angle
μ	=	Euler-Cauchy oscillation growth exponent
ν	=	Euler-Cauchy frequency coefficient
ρ	=	atmospheric density
τ	=	lag time factor
Subscripts		
eq	=	equivalent
∞	=	freestream
0	=	initial quantity
Superscripts		
AB	=	aftbody contribution
FB	=	forebody contribution
*	=	reference value for aftbody moment curve

I.   Introduction

ATMOSPHERIC entry is a critical phase for missions which seek to return astronauts or scientific payloads back to Earth or explore the surface of a body with an appreciable atmosphere. As a blunt vehicle enters a planetary atmosphere, the aerodynamic moments acting upon it can result in unstable pitching motions and divergence of oscillation amplitude. These instabilities typically arise just prior to maximum dynamic pressure and peak in the low or mid supersonic regime of the trajectory just prior to parachute deployment [1]. Characterizing the dynamic stability performance of an entry configuration is an area of research that has been plagued with experimental difficulties, contradictory observations, and large uncertainties [2]. Accompanying uncertainties in the expected dynamic response is a general lack of understanding regarding the flow physics that govern this complex phenomenon. As the paradigm for aerodynamic decelerators shifts from the rigid aeroshells used over the past half-century to more unfamiliar configurations such as inflatable decelerators which are being developed for utilization on future missions seeking to improve landed mass capability, there is added importance to understanding the mechanism by which dynamic instabilities arise and finding a means to rapidly and reliably quantify them.

Throughout the experimental history of dynamic stability investigations, it has been observed that the pitching moment often tends to exhibit a dependence on the direction of the pitching motion [3]-[6]. This type of hysteresis has been attributed to a phase lag between the aftbody and forebody pressure fields (and therefore pitching moment contributions). In the past decade, work has been conducted to investigate the possible means by which flow structures surrounding the blunt body can manifest into unsteady aftbody moments and, subsequently, oscillation divergence. Studies by Teramoto et al, [4] Abe et al, [5] and Schoenenberger [7] have shed light on and given credibility to this theory.

In order to further investigate the possible implications of a hysteresis effect on the aftbody contribution to the pitching moment and subsequent oscillation behavior, this study develops a governing model of the pitch dynamics through implementation of a time-lagged of the aftbody pitching moment. After developing this model, a parametric sweep is conducted on the variables relating to the time delay, amplitude, angle of attack dependence, and Mach number dependence of the aftbody pitching moment to identify values for these that parameters result in favorable

damping or cause oscillation divergence. These findings are then related to an equivalent pitch damping sum for comparison with the current formulation of the problem. The model is then used to reconstruct simulated ballistic range data and coupled with parameter estimation techniques, thereby demonstrating that combinations of the parameters governing the time-lagged pitching moment behavior can reproduce observed pitching behaviors without use of the pitch damping sum.

The possibility of finding a set of governing principles regarding the dynamic stability of blunt bodies that is not reliant on the pitch damping sum also leads to questions regarding the physical relevance of the coefficients which produce the pitch damping effect. If an equivalent response can be attained by using the formulation postulated here, perhaps the notion of the pitch damping sum is unnecessary and has served as a placeholder for the hysteresis in the aftbody pitching moment.

Although the standard description of pitch dynamics for entry vehicles does an adequate job of modeling a blunt body system, no reliable computational techniques exist to predict the key parameter for this model (the pitch damping sum) and the experimental methods for identifying this parameter are complex, expensive, and carry large uncertainties. Furthermore, the physical significance of the pitch damping sum is convoluted and non-intuitive. By developing a model which is independent of the pitch damping sum and instead relies on quantities which are both easier to measure or calculate computationally and have physical significance, the potential benefits of the model identified in this study are far-reaching for entry vehicle dynamics. As such, this work represents a first step towards development of an improved understanding of the governing physics of dynamic instability, and provides a more efficient and intuitive means of characterizing the dynamic behavior of entry vehicles.

II.   Pitching Moment Hysteresis of a Blunt Body

Experimental observations citing the importance of unsteady aftbody pressure fields on the pitch dynamics of blunt bodies are the driving motivation behind this work. As a body is pitching during its deceleration through the atmosphere, pressure changes on the forebody result in changes in the pitching moment contribution from the forebody. Similarly, the aftbody pressure field changes in time as the attitude of the vehicle changes.
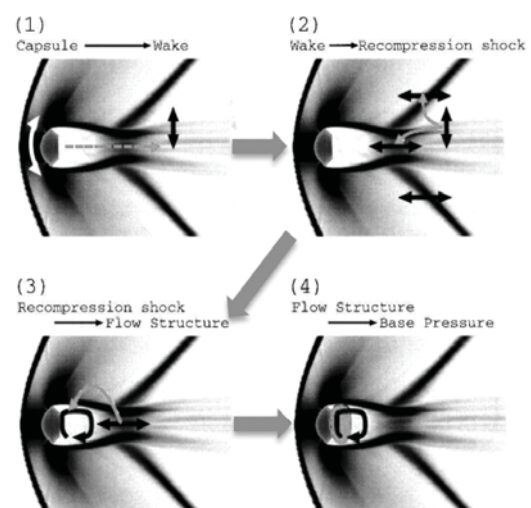

Fig. 1 Proposed sequence of events as the mechanism governing dynamic stability.[4]

However, changes in the aftbody pressure field, and thus the pitching moment contribution of the aftbody, are delayed by some finite time relative to the forebody. This time lagged response of the aftbody pressure field has been observed both experimentally and numerically [4], [6].

The duration of the delay is dependent on the physical mechanism by which pressure information in the flow is transmitted to the aftbody. One possible means by which this transmission occurs was proposed by Teramoto et al in a study where they tracked the position of the recompression shockwave and its time delay relative to the pitching motions [4]. It was determined that the base pressure fluctuations within the recirculation region were associated with the behavior of the recompression shockwave. Wang et al suggested a similar connection between the oscillation of a body and the motion of the rear stagnation point [8]. The behavior of the recompression shockwave seemed to be dictated by the behavior of the wake downstream following the convection of disturbances due to pitch oscillations.

The mechanism proposed by Teramoto et al is depicted in Fig. 1 and can be broken down into four steps: propagation of upstream disturbances due to pitching motions, modification of the wake downstream, motion of the recompression shock, and changes in the flow structure and base pressure within the recirculation region [4]. Each of the steps within this sequence has some finite time delay associated with it due to finite convection speeds within the flow. Combined, these time delays are responsible for the time lag seen in the base pressure and result in the observed hysteresis in the pitching moment. Computational pressure calculations from the work of Teramoto et al show the time delay of the aftbody pressure relative to changes in angle of attack and forebody pressure as well as the resulting pitching moment hysteresis of the Muses-C (Hayabusa) capsule (Fig. 2) [4].
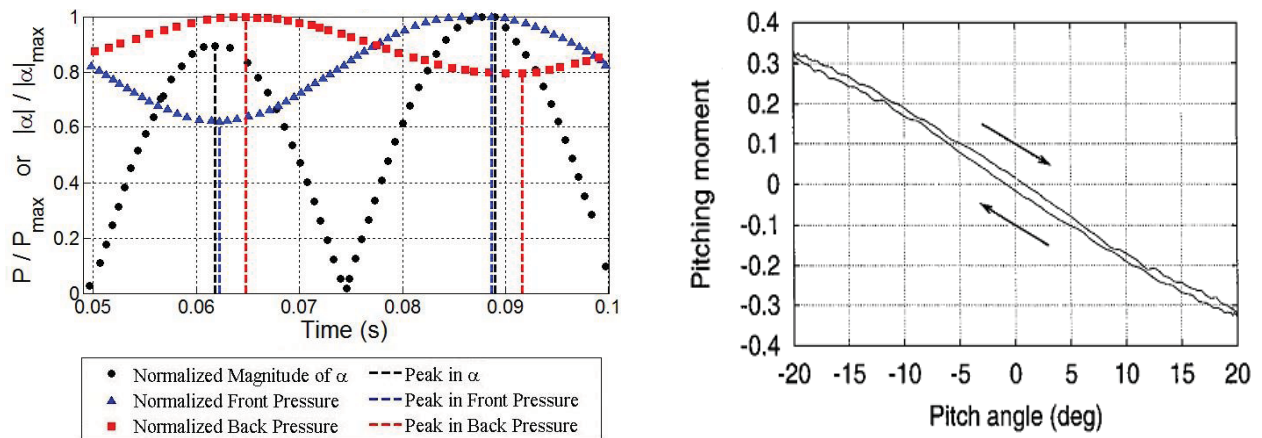
Fig. 2 Pressure variation with pitching motion (left, adapted) and corresponding hysteresis in pitching moment (right).[4]

Teramoto's results show that the front pressure adjusts almost instantaneously as the angle of attack oscillates, however, oscillations in the pressure field on the back of the vehicle lag by approximately 2 ms. The corresponding hysteresis loop in the pitching moment results in a net input of work to the system over each oscillation cycle and this influx of energy may be responsible for dynamic instabilities [3], [5] :

$$W = \frac{1}{2}\rho K_\alpha^2 A d \int_{(-\theta)+1} C_m d\theta \tag{1}$$

III.   Methodology

A. Standard Formulation of the Equations of Motion

The equations of motion that govern atmospheric entry trajectory of a blunt body are discussed thoroughly in the literature. Derivations of the equations typically assume planar motion and aerodynamic derivatives which are independent of Mach number and vary linearly with angle of attack [9]-[13]. These simplified equations of motion neglect rotational and gravitational effects and are only valid for low L/D vehicles flying at small angles of attack ($\alpha < 30^{o}$) [9]. The governing equations for the altitude, velocity, flight path angle, and pitch angle are given below:

$$\frac{dh}{dt} = \dot{h} = V\sin\gamma \tag{2}$$

$$\frac{dV}{dt} = \dot{V} = \frac{-\rho V^2 C_D S}{2}\frac{}{m} - g\sin\gamma \tag{3}$$

$$\frac{d\gamma}{dt} = \dot{\gamma} = \frac{\rho V S C_L}{2m} - \left(\frac{g}{V} - \frac{V}{R_e + h}\right)\cos\gamma \tag{4}$$

$$\frac{d^2\theta}{dt^2} = \ddot{\theta} = \frac{\rho V^2 S d}{2 I_{yy}}\left(C_{m_q}\frac{\dot{\theta}d}{2V} + C_{m_\alpha}\frac{\dot{\alpha}d}{2V} + C_{m_\alpha}\alpha\right) \tag{5}$$

Applying a few additional simplifying assumptions to Eq. 5, a closed form second order differential equation describing the time dependent behavior of the angle of attack oscillations can be attained [9] :

$$\ddot{\alpha} - \frac{\rho V A}{2m}\left[-C_{L_\alpha} + \frac{md^2}{2I}(C_{m_q} + C_{m_\alpha})\right]\dot{\alpha} - \frac{\rho V^2 A d}{2I}C_{m_\alpha}\alpha = 0 \tag{6}$$

Eq. 6 represents the traditional formulation of the dynamic pitching motion and will serve as the baseline description to which the results in this study will be compared. When all of the parameters for this standard formulation of the pitch dynamics are known, it does an excellent job of predicting the resulting dynamics of a vehicle. However, the

American Institute of Aeronautics and Astronautics

pitch damping sum $\left(C_{m_q} + C_{m_{\dot{\alpha}}}\right)$ is difficult to quantify and non-intuitive in nature. The resulting uncertainty in the pitch damping sum is detrimental to vehicle and mission design, as it is responsible for the growth rate of the pitch oscillations. The time-lagged aftbody pitching moment model developed in the following section seeks to describe the dynamics with more intuitive and tangible parameters than the pitch damping sum, thus allowing for more accurate and efficient prediction of the pitch dynamics of a vehicle while providing some insight into the driving mechanisms behind dynamic stability of blunt entry vehicles.

B. Time-Lagged Aftbody Pitching Moment Model

1. Form of the Aftbody Pitching Moment Curve

   To investigate the dynamic stability implications of an unsteady aftbody pitching moment experiencing hysteresis with respect to the pitching motion, a new model to describe the pitching moment of decelerating blunt bodies was developed. This model is applicable to simulating free-oscillation wind tunnel tests, ballistic range tests, and actual entry trajectories. As in the studies of Abe et al [5] and Schoenenberger [7], the approach is based on separating the forebody and aftbody contributions to the total pitching moment of the body:

$$^{Total}C_m = {}^{FB}C_m + {}^{AB}C_m \tag{7}$$

   The total pitching moment coefficient can be obtained via experimental data, CFD tools, or approximated with Modified Newtownian impact methods and is typically linear with angle of attack. A negative slope of the total pitching moment coefficient versus angle of attack corresponds to a statically stable configuration which will generate restoring moments following a perturbation. As the contribution to the pitching moment from the aftbody is generated by the unsteady pressure field of the recirculation region beyond the shoulder of a blunt vehicle, it can be periodic both temporally and with respect to angle of attack [4], [6]. This behavior was noted in the investigations of he hysteresis effects on dynamic stability by Beam and Hedstrom [3]. Fig. 3 displays both experimental (extracted from rear pressure measurements) and computational data for the MUSES-C capsule from Abe [5], and computational data generated with the CFD tool LAURA for the MER and Viking configurations by Schoenenberger [7]. These data sets show the angle of attack dependence of the aftbody pitching moment. Key features of these curves are: zero moment contribution at an angle of attack of zero, a global peak in the pitching moment between 5-10° followed by a small local minimum, and a second smaller peak at a high angle of attack.

Sensitivity studies showed that the response of the vehicle was relatively insensitive to the amplitude and location of
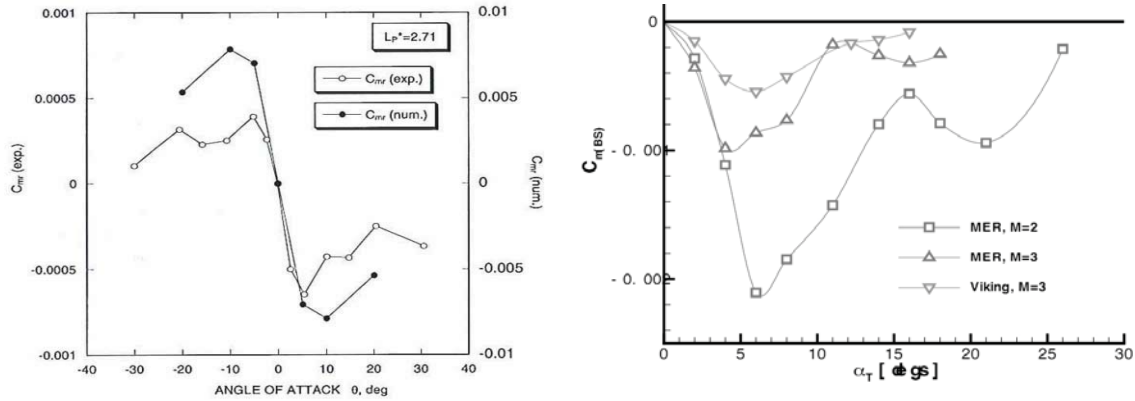
Fig. 3 Aftbody pitching moment vs. angle of attack from Abe[5] (left) and Schonenberger[7] (right)

the second peak. Additionally, the angle of attack where the second peak is located approaches the limit where the

small angle assumption inherent to equations of motion and the theory of the aftbody recirculation being the primary

mechanism causing the aftbody moments begins to break down. Thus, the peak amplitude of the aftbody moment

$(^{AB}C_m^*)$ and the angle of attack corresponding to this peak (α^*) were identified as the two key parameters by which

the shape of the aftbody moment curve would be defined. In the proposed model, the location and amplitude of the

second peak were held constant to reference values from the MER curve from Schonenberger [7] (equal to 1.25×10^{-3}

at M=2 and 20°, respectively). The local minimum was set to a value of 0.625×10^{-3} and occurred at an angle of attack equidistant from the value of α^* and the location of the second peak, 20°. Finally, the model was restricted to be symmetric for negative and positive angles of attack about an angle of attack of zero.

Further, the MER data from Schonenberger shows a significant Mach number dependence with approximately the same angle of attack dependence [7]. This observation is consistent with literature which suggests that the pitching moment coefficient has a
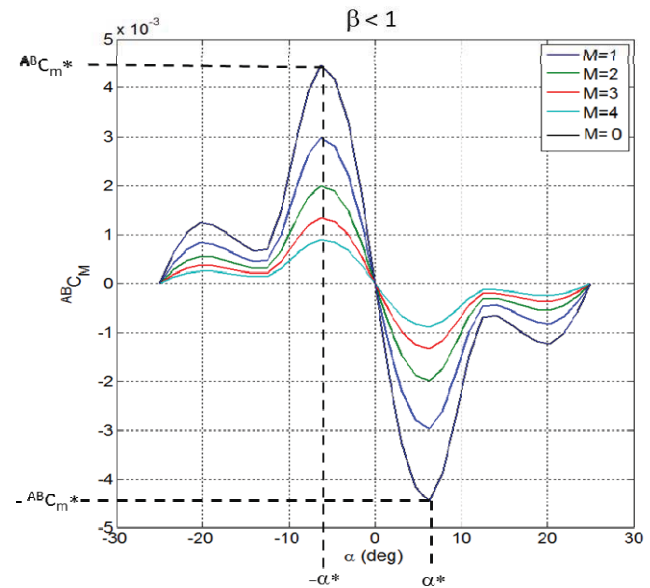
Fig. 4 Aftbody moment curve as defined by the three parameters: α^*, $^{AB}C_m^*$, and $\beta<1$

derivative with respect to velocity [14]. To account for the Mach number dependence, an additional parameter was introduced to fully define the aftbody moment contribution at all angles of attack and Mach numbers. This parameter (β) is a constant which scales the $^{AB}C_m$ at each angle of attack by the Mach number via a power law relation:

$$^{AB}C_m = \beta^M \, ^{AB}C_m^{*}$$

(8)

The parameter β incorporates the Mach number dependence of the pitching moment. Values less than one indicate that the amplitude of the pitching moment curve decreases with increasing Mach number. Similarly, if β is greater than one, the amplitude grows with increasing Mach number. A value of unity corresponds to an aftbody pitching moment curve which is independent of Mach number. Using this definition of β, the value of $^{AB}C_m^{*}$ corresponds to a reference $^{AB}C_m$ at a Mach number of zero. A representative set of the aftbody pitching moment data using this parameterization is shown in Fig. 4.

2. Time Lag

Differentiating the forebody and aftbody pitching moment contributions with respect to angle of attack yields:

$$^{AB}C_{m_\alpha} = \frac{\partial(^{AB}C_m)}{\partial\alpha}$$

(9)

$$^{FB}C_{m_\alpha} = \frac{\partial(^{FB}C_m)}{\partial\alpha} = \, ^{Total}C_{m_\alpha} - \, ^{AB}C_{m_\alpha}$$

(10)

Notice in Eq. (10) that the forebody moment slope is not explicitly defined as a constant, but is set equal to the difference of the total pitching moment coefficient slope and the aftbody contribution to maintain a constant total pitching moment coefficient slope. With a pitching moment slope coefficient defined as a function of Mach number for a wide range of angles of attack, the equations of motion can be integrated from the initial flight conditions of the vehicle to some terminal state. An ordinary differential equation solver (such as *ode45* in MATLAB) is insufficient for propagating this formulation of the equations of motion, as the pitch dynamics rely on not only the current state of the vehicle, but also some previous state at an earlier time ($t^- = t-t_{lag}$). Therefore, to implement the time lag of the aftbody response with respect to changes of the forebody pitching motion, a delay differential equation solver should be utilized (within MATLAB, *ddesd*). The value of t_{lag} can be constant, or defined by some function which is problem and state dependent. From Teramoto et al, it is clear that there exists some characteristic

parameters within the system that govern the resulting lag of the aftbody moment contribution.[4] For this study, the value of t_{lag} was defined by the ratio of a characteristic length and a characteristic velocity multiplied by a lag time factor, τ:

$$t_{lag} = \tau \frac{l}{v} \qquad (11)$$

This is akin to the reduced frequency parameter defined in many studies of dynamic stability [8],[15]-[17], but the value of τ scales this parameter to account for a possible increase in the length scale or decrease in the characteristic velocity. The hysteresis of the pitching motion and the subsequent oscillation growth of the vehicle are dependent on the factor τ and its influence is discussed in following sections. Historically, the characteristic length and time scales used to describe this phase lag and the dynamic behavior of a blunt body were the maximum diameter (or radius) of the vehicle and the freestream velocity [18]. Abe et al suggested that the characteristic length and velocity scales that govern the hysteresis effects are related to the flow in the wake region [5]. Specifically, Abe et al proposed that the characteristic length should be twice the maximum diameter of the vehicle and the characteristic velocity equal to half of the freestream value. Teramoto et al concluded from their study that the length scale was governed by the distance to the recompression shockwave ($\approx 4d$) and the characteristic velocity was the approximate convective velocity within the shear layer of the wake ($\approx 0.5\,V_\infty$) [4]. Large values of τ indicate that the length scale which governs the lag time are larger than the diameter of the vehicle, the propagation velocity of the forebody pressure changes to the aftbody is less than the freestream velocity, or some combination of these two effects. For example, using Teramoto's proposed characteristic length and velocity of 4d and $0.5\,V_\infty$, respectively, the lag time factor, $\tau = 4/0.5 = 8$.

3. Governing Equations With The Time-Lagged Aftbody Pitching Moment

Using this time lag concept combined with separation of the contributions of the forebody and aftbody to the total pitching moment coefficient, a new formulation of the pitching dynamics is postulated:

$$\ddot{\alpha}(t) - C_1 \dot{\alpha}(t) + C_1 \left[{}^{FB}C_{m_\alpha} \alpha(t) + {}^{AB}C_{m_\alpha}^- \alpha(t^-) \right] = 0 \qquad (12)$$

where:

$$ {}^{AB}C_{m_\alpha}^- = {}^{AB}C_{m_\alpha}(t^-) = {}^{AB}C_{m_\alpha}(M(t), \alpha(t^-)) \qquad (13)$$

and:

$$C_1 = \frac{\rho V A}{2m} C_A \qquad \text{and} \qquad C_2 = \frac{\rho V^2 A d}{2I} \qquad (14)$$

This formulation is a function of the environmental conditions, the mass properties of the vehicle, the axial force coefficient, the forebody pitching moment slope at the current time step, and the aftbody moment at time $t = t^-$. Note the absence of the pitch damping sum coefficient from this formulation. Instead, it is the time-shifted sampling of the angle of attack by the aftbody which creates a hysteresis in the pitching moment (C_m) and pitching moment slope ($C_{m\alpha}$) curves which govern pitch oscillation growth. At each time step within the *ddesd* integration of the equations of motion, an interpolation is done to determine the appropriate $^{AB}C_{m\alpha}$ for the current state of the vehicle, based on the state at t=t⁻.

Fig. 5 displays an example of the time history of the angle of attack of the vehicle as well as the shifted angle of attack sampled by the aftbody (due to the time lag). Notice that the lag time grows almost exactly linearly with time.
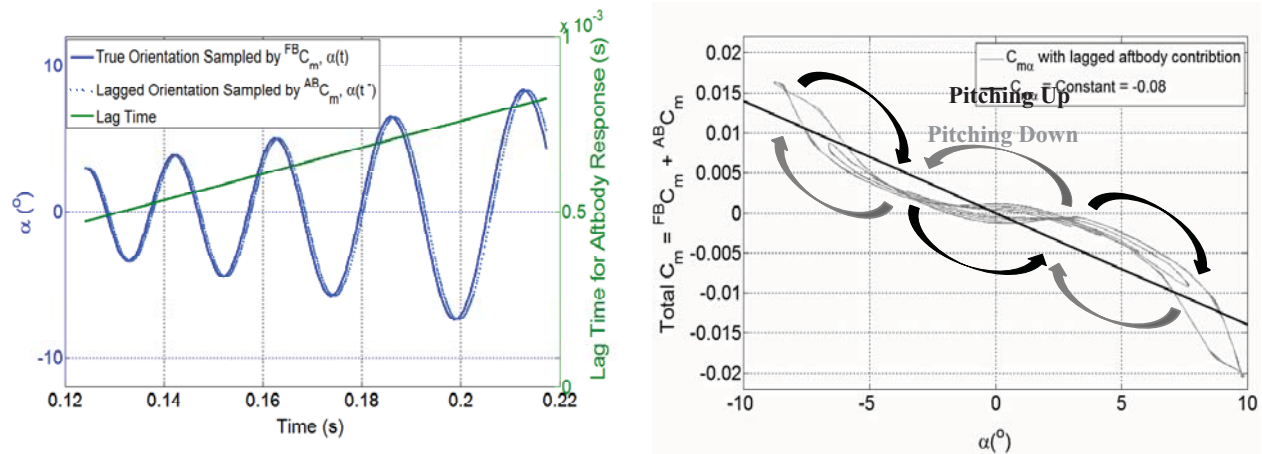

Fig. 5 True and lagged responses of pitching motion for the associated lag time (left) and the resulting hysteresis in the total pitching moment coefficient versus angle of attack (right)

This is because the velocity drops approximately inversely proportional to time (i.e. V(t) ∝ 1/t) and the time lag is

proportional to the inverse of the velocity. Also plotted are both the static and lagged curves for the total pitching

moment coefficient with respect to angle of attack. The static curve has a constant slope and a typical result of the

total pitching moment slope throughout the trajectory from the baseline equations of motion would lie on this line

due to the lack of the hysteresis effect. The lagged response exhibits both nonlinearities (due to the contribution of

the non-linear aftbody moment coefficient) and significant hysteresis during each pitch cycle. As τ increases, the

area enclosed within the pitching moment coefficient curve due to hysteresis increases, causing increased energy

addition to the pitching motion.

IV.   Results

A. Dynamic Excitation Analysis

With the model described in the previous section, the effect of the aftbody pitching moment and the hysteresis associated with it were investigated to examine the resulting oscillatory behavior for various combinations of the
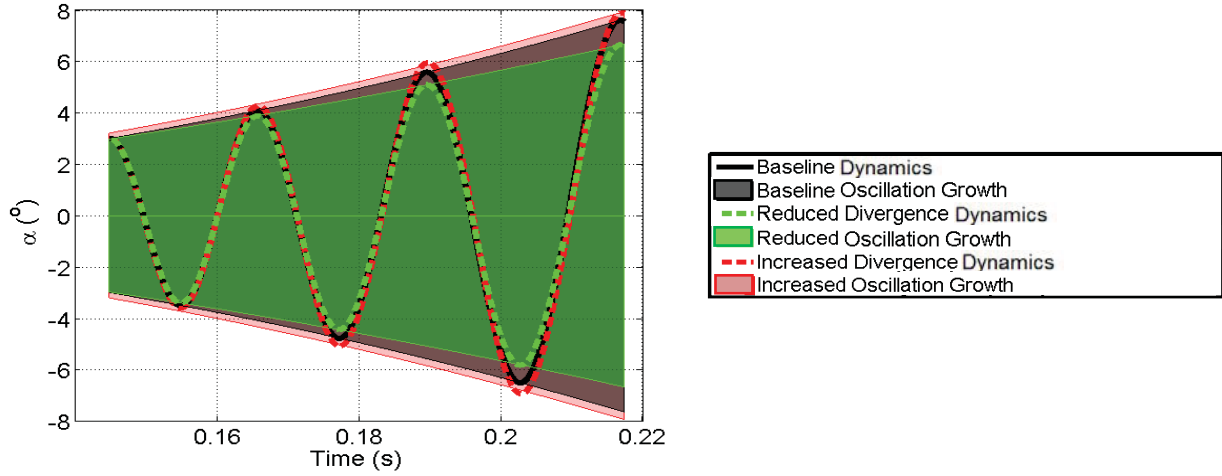
Fig. 6 Examples of reduced and increased oscillation divergence relative to a baseline trajectory

four governing parameters. From this, insight is gained about which combinations excited or impeded the dynamic response relative to a baseline case having the same mass properties and static aerodynamic characteristics, but using the traditional pitch damping description of dynamic stability. These results can provide insight pertaining to the governing physics of dynamic stability, such as the flow structures (characteristic size and velocity of the flow) which are most closely coupled to observed dynamic behaviors. Fig. 6 illustrates example cases with reduced and increased oscillation growth found using the model proposed in this study relative to the baseline dynamics.

The expected baseline response can be found numerically by propagating the baseline equations of motion and looking at either the maximum angle of attack reached during the trajectory or the growth rate of the oscillation peaks. The growth rate can also be predicted analytically for a given vehicle using the relation derived by Schonenberger as the solution to the Euler-Cauchy equation:[9]

$$\alpha = A t^\mu \cos(\nu \ln(t) + \delta) \qquad (15)$$

where:

$$\mu = \frac{md^2 \left(C_{m_q} + C_{m_{\dot\alpha}} \right)}{4 I_{yy} C_A} \qquad (16)$$

The growth rate for the response generated by the time-lagged aftbody moment model for dynamic stability proposed in this study was found by fitting the observed peaks and their corresponding times with a power law:

$$\alpha_{peak} = A t^{\mu_{fit}/2}$$ (17)

From this fit, an "equivalent effective C_{mq} response" was determined by rearranging Eq. 16 and using the value of the growth exponent determined by the fit, μ_{fit}:

$$\overline{C_{mq_{eff}}} = \frac{\mu_{fit} 4 I_{yy} C_A}{m d^2}$$ (18)

This is the response generated by the time lagged aftbody pitching moment model which produces an equivalent oscillation growth rate as the standard pitch dynamics model with a given value of $\overline{C_{mq}}$.

*1. Case Study: Mars Exploration Rover Ballistic Range Model*

For a vehicle with given static aerodynamics and mass properties, the four parameter design space for generating dynamic responses using the model proposed in this study can be explored. To visualize the space, one parameter is fixed at various discrete values for which the other three can be continuously varied to generate a response. These responses can be viewed in either 2D contour slices of the space or through isosurfaces. There are various approaches to choosing the fixed parameter, but the most efficient scenario is to isolate the one for which there is some predetermined knowledge.

The design space exploration process will be demonstrated through a case study for a simulated ballistic range test for which the initial Mach number is 3.0, the terminal Mach

Table 1. MER Case Study Properties

Parameter	Value
M_0	3.0
M_f	2.0
α_0	3°
Diameter, d	.07 m
Mass, m	.584 kg
I_{yy}	kg-m²
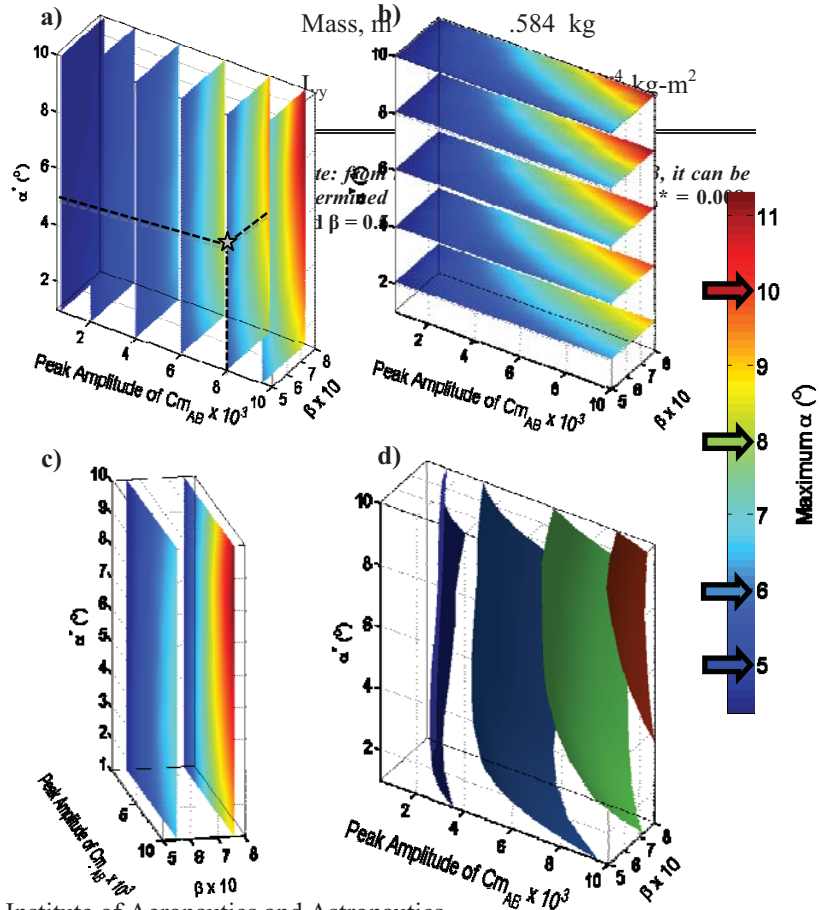
Fig. 7 Selected contour slices (a-c) and isosurfaces (d, indicated by arrows on the colorbar) for the maximum angle of attack reached of the MER ballistic range model with τ=8.0.
*Note: MER values are indicated on figure a) with a star
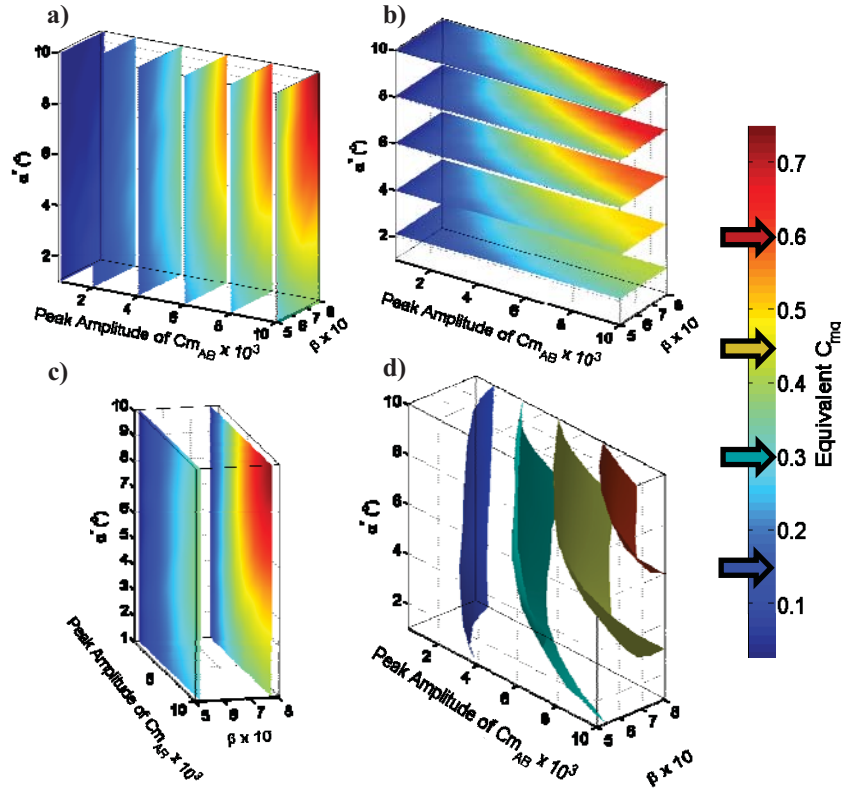
Fig. 8 Selected contour slices (a-c) and isosurfaces (d, indicated by arrows on the colorbar) for the equivalent pitch damping sum responses of the MER ballistic range model with τ=8.0
*Note: MER values are indicated on figure a) with a star

number is 2.0, and the initial angle of attack is 3 degrees. The vehicle has the mass properties and static aerodynamic characteristics of the MER ballistic range model that was used by Schonenberger et al for the dynamic stability testing of the MER aeroshell design (see Table 1).[18]

The parameter which was discretized and fixed in this example case is the time lag factor, τ. The time lag factor was set equal to 8.0, which is the value proposed by Teramoto et al.[4] Thus, by examining the rest of the design space, the validity of τ=8.0 can be assessed by subjectively determining if realistic responses can be produced with values of the other three parameters. Fig. 7 and Fig. 8 show the dynamic response in terms of maximum angle of attack and equivalent effective pitch damping sum, respectively. Displayed in these figures are contour slices in all three of the remaining parameter dimensions as well as isosurfaces at four discrete values of the two respective response measures (indicated by the arrows on the colorbar).

There exists a vast amount of information in Fig. 7 and Fig. 8 which can be useful for understanding dynamic instability and guiding vehicle development. In general, it can be seen that oscillation divergence increases strongly with the magnitude of the reference peak amplitude of the aftbody moment coefficient ($^{AB}C_m{}^*$) and the Mach number dependence of the aftbody moment (β). Divergence also increases weakly with increasing angle of attack of peak aftbody moment, α*, with a maximum occurring between 6° and 10°. If one can find a means of controlling

the amplitude of $^{AB}C_m{}^*$ (say, for example, through geometry modifications to alter the flowfield) then an upper bound on the angle of attack divergence may be estimated, even without additional knowledge about α^* or β.

Another key observation regarding the data in Fig. 7 and Fig. 8 is that, within the three free parameters, there exists a three-dimensional surface of values of which can produce a given response. Taking into account the fact that a three-dimensional surface exists

Fig. 9 Maximum angle of attack and equivalent Cmq responses of the MER ballistic range model with τ=8.0 and $^{AB}C_m{}^* = 0.009$.

for each possible value of the isolated parameter (in this case, τ), it is clear that the design space within this parameterization is multi-modal, having numerous non-unique solutions. The process of isolating individual parameters can be carried out in parallel, based on the information at hand, or sequentially where the design space is reduced with knowledge about additional parameters. If knowledge about a second parameter can be estimated experimentally or computationally, the possible values that the remaining two parameters can take to produce a particular response are reduced to lie on a line. This can be seen in Fig. 9 where the space is reduced to values of α^* and β for a given reference peak amplitude ($^{AB}C_m{}^*$). The more that is known about the possible values that the parameters can take, the further the design space for the dynamic response can be reduced.

The ability to visualize and understand the design space can be used not only for parameter identification purposes, but also to bound the parameters for a given response requirement. For example, consider a parachute staging scenario for an entry vehicle where parachute deployment is triggered by a specified velocity condition which should occur somewhere between Mach 3 and 2, depending on the atmospheric conditions. For a given upper bound on the possible angle of attack just prior to Mach 3 and some additional information about the vehicle (say τ and $^{AB}C_m{}^*$, as in the previous examples), the remaining design space can be used to inform aeroshell design. For example, if the maximum allowable angle of attack which can be tolerated between Mach 3 and 2 is restricted to 9$^{\mathrm{o}}$ (denoted by the white band in the left contour plot of Fig. 9), one could refer to information such as that presented in Fig. 9 to learn about the allowable values of α^* and β, which may be connected to the aeroshell geometry and make
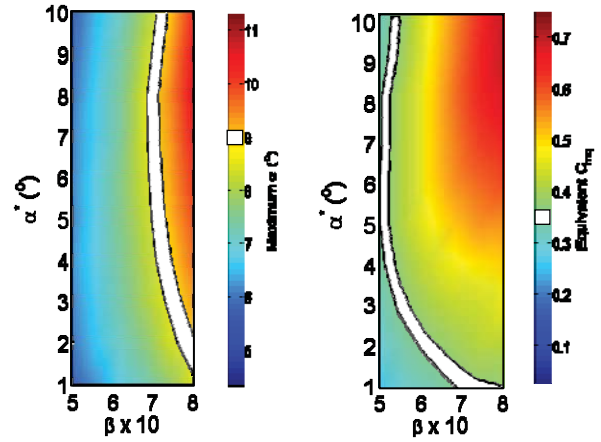
design choices appropriately. In this example, it can be seen that for these conditions the response is not strongly dependent on α^* and β must be approximately < 0.75 for all $\alpha^* > 3^o$ for the maximum angle of attack to not exceed 9°.

This exercise can be performed in terms of a desired (or maximum allowable) equivalent C_{mq} response as well, as shown on the right of Fig. 9 where the highlighted band of $C_{mq}=0.35$ traces a line through α^* and β space showing values which result in the specified response.

Knowledge about the parameters governing the dynamic model defined in this study can be useful in vehicle design in addition to providing further understanding of dynamic stability. However, means to obtain the information required to reduce the parameter space to a manageable size are not specified. The next section will examine the use of trajectory reconstruction techniques to estimate these parameters with a series of ballistic range shots.

B. Trajectory Reconstruction Analysis for Experimental Validation of Proposed Model

Experimental validation of the proposed model via ballistic range testing would add confidence to the formulation of the problem. Once validated, this model could then be utilized in future studies to quantify the expected dynamic response of vehicles without the need to quantify the pitch damping sum. Such an experiment is outside the scope of this study. However, a simulated ballistic range test campaign was conducted to assess the

Fig. 10. Representative simulated and reconstructed trajectories with residuals

$$\varepsilon_i^2 = \left(\alpha_{\text{Reconstruction, i}} - \alpha_{\text{Sim, i}}\right)^2$$
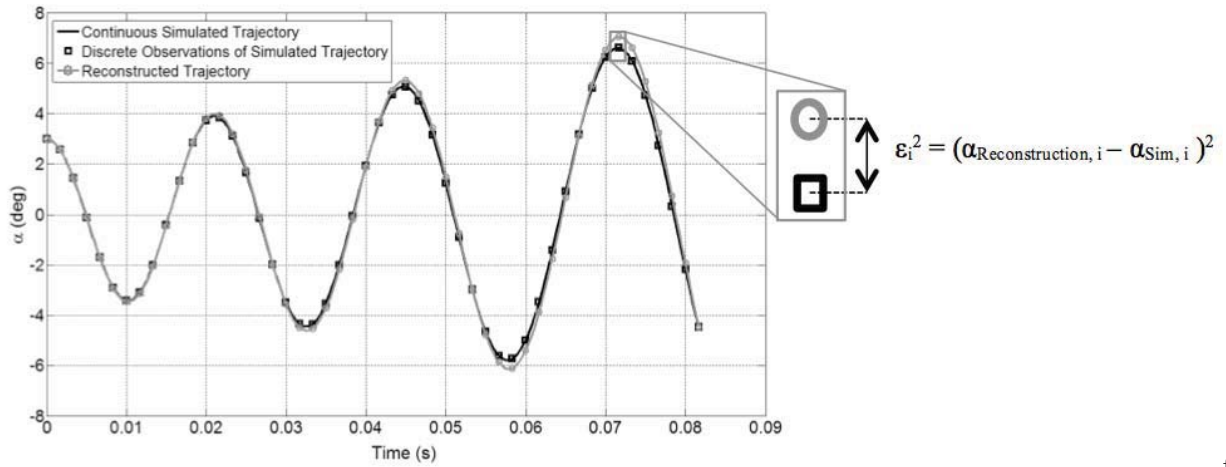
f

easibility of such an effort. A set of ballistic range trajectories were simulated using the baseline (standard) equations of motion with a fixed set of parameters. The data (angle of attack versus time) from these simulations is known to match the true dynamics well when perfect knowledge of the dynamic derivatives exists.[‡] Because ballistic range data is not a continuous data set, but instead comes from discrete observations using schlieren photography, the data from these simulations was discretized into 50 evenly spaced observations in time. Using the generated data set of 50 angles of attack observed at 50 corresponding times along the simulated ballistic range shots as a "truth", a genetic algorithm (GA) was wrapped around the time lagged aftbody pitching moment model to explore the parameter space to find a set of parameters which result in a trajectory that best matches the simulated experimental data. A GA was utilized over gradient based methods because of the multi-modal nature of the parameter space.

The reconstruction was optimized in a least squares sense, with the sum of the square of the residuals at each of the 50 observation points in time as the objective function (see Fig. 10 and Eq. 19):

$$J = \sum_{i=1}^{50} \varepsilon_i^2 = \sum_{i=1}^{50} \left(\alpha_{\text{Reconstruction}}(t_i) - \alpha_{\text{Simulated}}(t_i)\right)^2 \tag{19}$$

The GA was used to identify the four parameters which best fit the simulated ballistic range data using the same MER ballistic range vehicle specified in Table 1 with various initial conditions (angle of attack and Mach number). The ranges of initial conditions which were explored represented those typical of ballistic range test campaigns and

---

[‡] Recall that one of the primary motivations for the development of the model proposed in this study is the fact that quantifying these derivatives is difficult and has large uncertainties.

therefore focused on initial Mach numbers in the low to mid supersonic regime with low to moderate initial angles of attack. The terminal Mach number for all cases was 2.0. Four different scenarios with different sets of initial conditions were considered with an increasing number of points that filled in the initial condition space to different degrees (see Fig. 11). The two trajectory case (N=2) utilized only the two extremes of initial condition combinations to use for the parameter estimation. Points were added to the two remaining corners of the space for N=4 and at the midpoint of each edge as well as the center for the N=9 case. Finally, points were added within the interior of the space, equidistant from all other neighboring points in the fourth scenario (N=13).
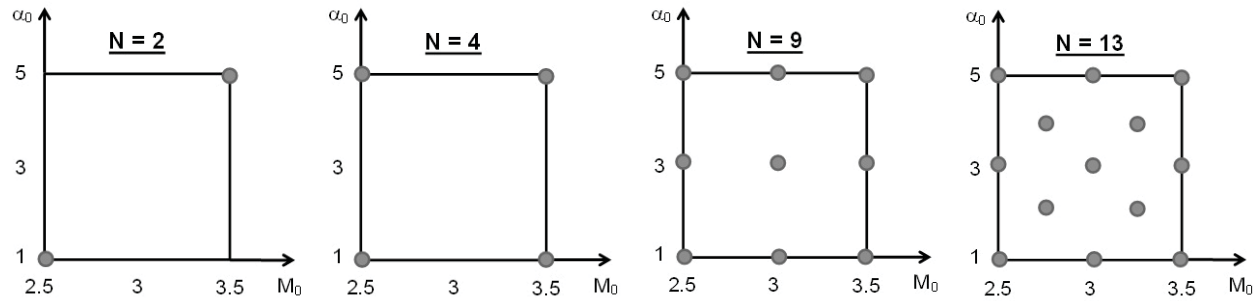
Fig. 11 Initial Mach numbers and angles of attack used for the four different test cases

In an attempt to ensure that the best fitting set of parameters was found for each case, the GA was run until convergence 32 times for each scenario, thus producing a statistically significant sample from which a mean could be taken. The means of all four parameters for each case are shown in Table 2.

Table 2. Mean parameter values with 32 GA runs for each case

Parameter	Number of Trajectories			
	N = 2	N = 4	N = 9	N = 13
τ	8.365	8.016	7.976	7.321
β	0.763	0.746	0.727	0.736
α^* (°)	6.931	7.281	7.278	7.281
$^{AB}C_m^* \times 10^3$	6.137	5.759	5.592	5.704

The estimated parameters seem to match up well with the limited literature that is available to anchor this analysis. The estimates for the time lag factor are very near to the value proposed by Teramoto et al of $\tau = 8$.[4] This adds credibility to their theory of the dominating length scale being the approximate distance to the recompression shock and the characteristic velocity being approximately half of the freestream value. Additionally, it can be seen in Fig. 13 that although the magnitudes are larger, the shape of the aftbody moment coefficient curves defined by the N=13 case closely

Fig. 12 MER aftbody moment coefficient versus angle of attack as estimated using N=13 and calculated using LAURA. [7][7]

match the LAURA estimates found by Schoneneberger.[7] It also can be seen from Table 2 that for the MER vehicle in the range of conditions examined, the four parameters converge to quite similar values in all four scenarios. This poses the following question: how many trajectories within the given initial condition space are required to accurately identify the parameters which can represent trajectories for the entire space? To test this, the average error for each of the 50 observed data points was calculated using the parameters found with all four test campaign scenarios (N=[2,4,9,13]). The average errors were calculated by taking the set of parameters found with a given test case (N) and then comparing the resulting trajectories to the baseline case at all of the exterior points as well as the center point of the initial condition combinations (see Fig. 12). In general, the model can reconstruct the original trajectories very well, with an average error of less than 0.4^o for almost all scenarios. Fig. 12 demonstrates that the average error is reduced as the number of ballistic range shots increases, with a majority of the error removed when N>4.

Some sets of initial conditions produce higher average errors than others. This is expected, as the trajectories with higher average error are those that grow to larger oscillation amplitudes due to the initial conditions, so the absolute error also grows. The two exceptions are for the cases with an initial angle of attack of 5° and initial Mach numbers of 3.0 and 3.5. With $\alpha_0 = 5^o$ and $M_0 = 3.0$, the error reduces significantly from N=2 to N=4, but then plateaus as N increases. For the most extreme case of the initial condition combinations ($\alpha_0 = 5^o$, $M_0 = 3.5$), the error actually grows with the number of trajectories. This is a result of the GA seeking to reduce the least square error for
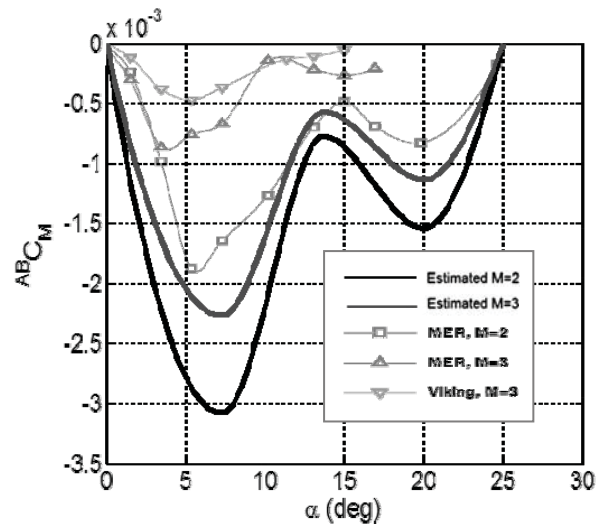
American Institute of Aeronautics and Astronautics

20

the entire array of cases. As the number of shots increases, the GA begins to favor solutions which are most applicable to the entire space. As such, the influence of the most extreme case diminishes and thus the final solution performs poorly at that condition.

Results like those shown in Fig. 12 can be used to inform the design of a future experimental campaign. Fig. 12 shows that a modest number of ballistic range shots are required to obtain reasonable parameter estimates. A
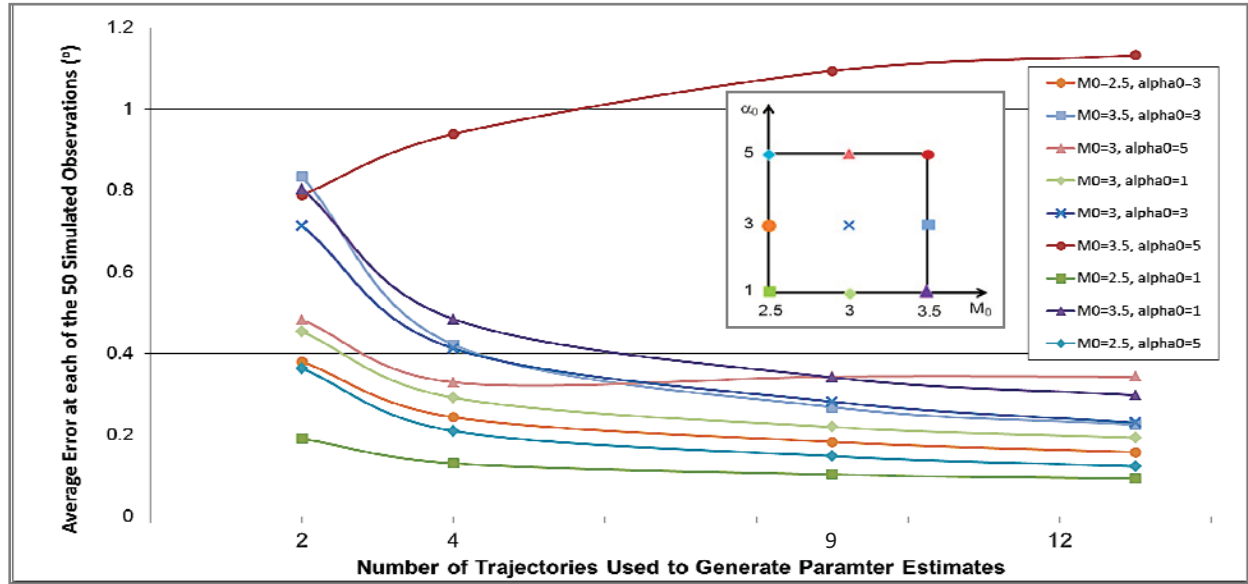
Fig. 13 Average error versus number of trajectories used to estimate the parameters at various initial condition combinations

ballistic range test campaign to identify these parameters would anchor the model proposed in this study and add fidelity to its definition of the problem and provide insight into the vehicle and flowfield characteristics which dominate dynamic stability. With this added confidence, this model could then be used without the need for ballistic range testing, but only a combination of CFD and less rigorous experiments to identify the parameters proposed in this study.

Eventually, the model proposed in this study (or one like it) should be capable of replacing the need for the use of the pitch damping sum in the description of blunt body dynamics entirely. Once fully developed, this approach of characterizing the stability of an entry vehicle has the advantage of being based on intuitive and physical quantities, such as the characteristic size and velocity of the wake flow and the pitching moment curve for the aftbody. All of these parameters could possibly be directly measured or estimated computationally.

V.   Summary

For the blunt vehicles utilized for atmospheric entry applications, the phenomenon of dynamic stability remains among the least understood. The current description of the pitch dynamics relies on quantification of the pitch damping sum coefficient which is time-intensive, non-intuitive, and carries significant uncertainty. As an alternative, a new model is proposed in this study building on earlier work [5],[7] to describe the pitching motions of a blunt vehicle without reliance on this coefficient. The driving force for oscillation growth in this new model is the aftbody pitching moment contribution which lags behind flowfield changes at the forebody due to finite convection of pressure information in the wake and boundary layer.

The new model introduces four parameters which fully describe the magnitude, angle of attack dependence, and Mach number dependence of the aftbody moment coefficient, as well as the time delay of their application relative to changes at the forebody. This new description of the pitch dynamics has the advantage of being more intuitive, physically grounded, and less demanding experimentally (or computationally). With this model, parametric sweeps were conducted across the four dimensional space to assess whether the magnitude of oscillation growth seen in real entry vehicles could be attained with physically realistic values of the parameters. It was found that the model can indeed replicate the types of oscillation divergence which are common to blunt body vehicles in supersonic flow.

Isolating one parameter at discretized values by assuming some *a priori* knowledge, isosurfaces containing values of three remaining parameters were identified. These surfaces represent non-unique solutions producing the same dynamic response. Isosurfaces and contour slices through the design space yield significant insight into the interactions of the parameters established here and the governing physics which are responsible for dynamic stability. This insight was shown to be useful in not only understanding the physics of dynamic stability, but as a design and analysis tool which can aid in scenarios such as parachute staging requirements and the design of future experimental test campaigns aimed at gaining a better understanding of supersonic dynamic stability.

There is little existing literature investigating any of the parameters which are critical to the model proposed in this study. As such, a ballistic range test campaign was simulated to help quantify the scale of such a test and the expected accuracy of the parameters which would be subsequently identified from the data. Parameter identification found evidence which supported the value for the time lag factor proposed by Teramoto et al[4] and the estimated aftbody moment curve was similar to one predicted computationally by Schonenberger.[7] If such a test were conducted to help validate the model, computational methods and simple experiments could be used to identify the

new governing parameters instead of (or as a complement to) ballistic range campaigns. If these methods were found to be more accurate and/or less exhaustive than those currently required for quantifying the pitch damping sum, the model proposed in this study may form the basis for replacing the standard formulation of the problem.

The results of this study have shed light onto the governing time scales of dynamic stability and the favorable and unfavorable aftbody pitching moment coefficients and then connected these observations to vehicle and mission design considerations. Further work comparing the results across a variety of vehicles with different known stability characteristics would better inform the model, eventually leading to an experimental campaign to quantify the parameters proposed in this study and unveil additional details behind the phenomenon of dynamic stability.

VI.   Acknowledgements

VII.   References

[1]   G. T. Chapman and L. A. Yates, "Dynamics of Planetary Probes⬚: Design and Testing Issues," *AIAA 1998-0797*, 1998.

[2]   C. D. Kazemba, R. D. Braun, I. G. Clark, and M. Schoenenberger, "Survey of Blunt Body Dynamic Stability in Supersonic Flow," *AIAA Atmospheric Flight Mechanics Conference, AIAA-2012-4509*, Aug 2012,

[3]   B. H. Beam and E. C. Hedstrom, "Damping in Pitch of Bluff Bodies of Revolution at Mach Numbers from 2.5 to 3.5," *NASA TM X-90*, Nov. 1959.

[4]   S. Teramoto, K. Fujii, and K. Hiraki, "Numerical Analysis of Dynamic Stability of a Reentry Capsule at Transonic Speeds," *AIAA 98-4451* and *AIAA Journal*, vol. 39, no. 4, pp. 646-653, Apr. 2001.

[5]   T. Abe, S. Sato, Y. Matsukawa, K. Yamamoto, and K. Hiraoka, "Study for Dynamically Unstable Motion of Reentry Capsule," *AIAA-2000-2589*, 2000.

[6]   K. Hiraki, Y. Inatani, N. Ishii, T. Nakajima, and M. Hinada, "Dynamic Stability of Muses-C Capsule," *21st International Symposium on Space Technology, ISTS 98-d-33*, 1998.

[7]   M. Schoenenberger, "Supersonic Pitch Damping Preditions of Blunt Entry Vehicles from Static CFD Solutions", Unpublished, 2003.

[8]   F. Y. Wang, J. M. Charbonnier, and O. Karatekin, "Low-Speed Aerodynamics of a Planetary Entry Capsule," *Journal of Spacecraft and Rockets*, vol. 36, no. 5, pp. 659-667, Sep. 1999.

[9]   M. Schoenenberger and E. M. Queen, "Limit Cycle Analysis Applied to the Oscillations of Decelerating Blunt-Body Entry Vehicles," *RTO-MP-AVT-152*, 2008.

[10] J. H. Allen, "Motion of a Ballistic Missile Angularly Misaligned With The Flight Path Upon Entering The Atmosphere and Its Effect Upon Aerodynamic Heating, Aerodynamic Loads, And Miss Distance," *NACA TN-4048*, 1957.

[11] M. Tobak and J. H. Allen, "Dynamic Stability of Vehicles Traversing Ascending or Descending Paths Through The Atmosphere," *NACA TN-4275*, 1958

[12] M. Baillion, "Blunt Bodies Dynamic Derivatives," *AGARD-R-808 – Capsule Aerothermodynamics*, 1995.

[13] B. Dayman Jr., J. M. Brayshaw Jr., D. A. Nelson, P. Jaffe, and T. L. Babineaux, "The Influence of Shape on Aerodynamic Damping of Oscillatory Motion During Mars Atmosphere Entry and Measurement of Pitch Damping at Large Oscillation Amplitudes," *JPL TR 32-380*, 1963.

[14] B. Etkin, Dynamics of Atmospheric Flight, John Wiley, New York (1972)

[15] F. Y. Wang, J. M. Charbonnier, O. Karatekin, and S. Paris, "The Utilization of Low Speed Facilities in Transonic Stability of Reentry Vehicles Research - An Evaluation," *AIAA 98-2636*, 1998.

[16] F. Y. Wang, J. M. Charbonnier, and O. Karatekin, "Low-Speed Aerodynamics of a Planetary Entry Capsule," *Journal of Spacecraft and Rockets*, vol. 36, no. 5, pp. 659-667, Sep. 1999.

[17] S. M. Murman, "Reduced-Frequency Approach for Calculating Dynamic Derivatives," *AIAA Journal,* vol. 45, no. 6, pp. 1161-1168, Jun. 2007.

[18] C. H. Whitlock and P. M. Siemers, "Parameters Influencing Dynamic Stability Characteristics of Viking-Type Entry Configurations at Mach 1.76," *Journal of Spacecraft and Rockets*, vol. 9, no. 7, pp. 558-560, Jul. 1972.

[19] M. Schoenenberger, W. Hathaway, L. Yates, and P. Desai, "Ballistic Range Testing of the Mars Exploration Rover Entry Capsule," *43rd AIAA Aerospace Sciences Meeting, AIAA-2005-55*, 2005.